(2)

AD-A264 339

MENTATION PAGE

Form Approved
OMB No. 0704-0188

2. REPORT DATE	3. REPORT TYPE AND DATES COVERED
	Final Report 01 Mar 90 - 31 Oct 92

4. TITLE AND SUBTITLE

Applications of the photorefractive effect and damage induced effects in fibers

5. FUNDING NUMBERS

AFOSR-90-0198

6. AUTHOR(S)

Professor Dana Z. Anderson

7. PERFORMING ORGANIZATION NAME(S) AND ADDRESS(ES)

Univ of Colorado
Department of Physics & Joint Institute for Laboratory Astrophysics
Boulder, CO 80309-0440

8. PERFORMING ORGANIZATION REPORT NUMBER

AFOSR-TR 93 0 [illegible]7

9. SPONSORING/MONITORING AGENCY NAME(S) AND ADDRESS(ES)

AFOSR/NE
110 Duncan Avenue Suite B115
Bolling AFB DC 20332-0001

10. SPONSORING/MONITORING AGENCY REPORT NUMBER

2301/AS

11. SUPPLEMENTARY NOTES

12a. DISTRIBUTION/AVAILABILITY STATEMENT

UNLIMITED

13. ABSTRACT (Maximum 200 words)

This is a final report of work carried out under AFOSR contract #AFOSR-90-0198. The focus is two-fold. One aspect concerns photoinduced effects in fibers, expecially the processes of self-organized second-harmonic generation in fibers. For the most part we have developed the microscopic theory of defect formation in glass. The basic physics involved in second-harmonic generation in fibers has led to a number other possible experiments and applications. For example, it is known that a photogenerated current cannot be produced by a single optical beam illuminating a centrosymmetic medium but it is now recognized that a current can be generated in a centrosymmetric medium by illumination with two harmonically related optical fields. However, we have concluded that as an application, self-organized second-harmonic generation in fibers does not appear to be a practical means of frequency doubling conventional lasers. Thus, until a conceptual or practical breakthrough occurs, we have brought to a close the experimental and theroetical work on this subject. (SEE REPORT FOR MORE DETAILS)

14. SUBJECT TERMS	15. NUMBER OF PAGES
	16. PRICE CODE

17. SECURITY CLASSIFICATION OF REPORT	18. SECURITY CLASSIFICATION OF THIS PAGE	19. SECURITY CLASSIFICATION OF ABSTRACT	20. LIMITATION OF ABSTRACT
UNCLASS	UNCLASS	UNCLASS	UL

Reversibility and Time Dependence of $\chi^{(2)}$ Grating Erasure in Optical Fibers

Baiming Guo, James Leitch, Anat Sneh, and Dana Z. Anderson

Department of Physics and Joint Institute for Laboratory Astrophysics
University of Colorado , Boulder, CO 80309-0440

Abstract

We performed a reversibility test of $\chi^{(2)}$ gratings in Ge-doped optical fibers to gain some insight into $\chi^{(2)}$ grating dynamics. The gratings were written with an IR beam and its second harmonic and erased with the second harmonic beam. No drop in the saturated second-harmonic power was seen for at least ten cycles of growth and erasure, indicating that grating formation is optically reversible. We also investigated the time dependence of the erasure and the change in the erasure rate with the erasing intensity. The grating amplitude shows a power law dependence on erasure time, in agreement with Ouellette et al. We show that the power law can be derived from a fundamentally exponential process through consideration of the near Gaussian transverse intensity profile of the fiber modes. Finally, we determine the number of 532 nm photons involved in the erasing process to be N = 3.8±0.2. We speculate that a metastable state may be responsible for such a large photon number.

PACS number:

Introduction

The mechanism of efficient second-harmonic generation in doped glass fibers has been investigated since Osterberg and Margulis observed efficient second harmonic generation in optical fibers in 1986.[1,2] By now, several models have been proposed,[3,4,5,6] and many researchers suggested that a defects-related self-organized periodic $\chi^{(2)}$ grating is responsible for the efficient second-harmonic generation, although the different models give different mechanisms for growth of the $\chi(2)$ grating. Some researchers have demonstrated optical erasure of $\chi(2)$ gratings and several have measured the photon number dependence at different wavelengths.[7-13] Ouellette et al.'s green light erasure experiment[7] suggested the time dependence of the erasure obeys $[I_{SH}(0) / I_{SH}(t)]^{1/2} \propto t$. They found a photon number of 4.2±1.2 at 532nm and stated that the process was reversible. Hibino et al.'s IR light erasure[11] gave 4.1±0.5 photons at 1064nm. Carvalho et al.'s UV light erasure[12] gave 1.2±0.2, an one UV photon process. Ehrlich-Holl et al.'s erasure experiment[13] showed that the growth/erasure process was irreversible in Ge- and P-doped optical fibers. We investigated the reversibility of the $\chi(2)$ gratings to obtain some insight into the dynamics of the gratings. We also characterized the time dependence of the erasure and the change in the erasure rate with the erasure intensity. Both the IR and its second harmonic are used for the seeded grating growth and only the second-harmonic beam is used for erasure of the grating after the saturated growth. We showed that the $\chi(2)$ grating seeded growth and subsequent green light erasure is reversible in Ge-doped single mode optical fibers, indicating that the microscopic grating formation/erasure process is evidently reversible. The grating amplitude showed a power law dependence on erasure time, in agreement with Ouellette et al.[7] We showed that the power law can be derived from a fundamentally exponential process through consideration of the transverse Gaussian intensity profile of the fiber modes. We also found the number of 532nm photons participating in the grating erasure process to be

3.8±0.2. We give a possible explanation based on the existence of a metastable intermediate state.

Experiments

The experimental setup is shown in Fig. 1. We used Newport F-SA fiber (single mode in green) having a Ge-doped core with a 3.2μm core diameter and an NA of 0.11. The 4.0cm-long fibers with well-cleaved ends were immersed in index matching fluid to exclude cladding modes. The 1064nm IR average power through the fiber was about 56mW, corresponding to a peak power of about 10kW for the mode-locked and Q-switched Nd:YAG laser pulses. The average seed power at 532nm was 0.75mW through the fiber. The erasure power at 532nm was in the range from 0.28 to 2.5mW. We prepared the grating by sending both the IR and the seed beams into the fiber until the induced second harmonic reached saturation and erased the grating using only the second-harmonic beam. Furthermore, the relative phase between the seed second-harmonic and IR writing beams is maintained with the help of an auxiliary SHG crystal and a phase-sensitive servo system. The phase servo includes a piezo phase adjuster, a KDP crystal, a photodetector, a lockin amplifier and a signal generator.

Results and Discussions

Our first experiment is to test the reversibility. We showed that the grating seeded growth/green light erasure process is reversible. We wrote and then erased the gratings to at least ten cycles in a single fiber with observing no drop in the saturated second-harmonic efficiency (Fig. 2). It indicated that the microscopic process involved is

evidently reversible. The reversibility also allows us to use a single piece of fiber for entire experiments.

We next determine the time dependence of the green light erasure. We found that the time dependence of the erasure is non-exponential, similar to the findings of Ouellette et al.[7] They suggested that the erasure of the grating amplitude G(t) is given by a power law

$$dG(t)/dt = -\alpha G^{x}(t)$$

assuming that the induced second-harmonic intensity $I_{SH}(t)$ is proportional to $G^2(t)$, then the time dependence of the second-harmonic intensity is given by

$$I_{SH}(t) = I_{SH}(0)/[1 + 2I_{SH}^{x}(0)x\alpha t]^{1/x} \qquad (1)$$

where α is the erasure rate, x is a parameter reflecting the time dependence The time dependence erasure exponent x and the erasure rate α are both free parameters in our fit. Our experimental data fit well by the power law, as shown in Fig. 3. The time dependence can be explained by examining the influence of a *non-uniform intensity* profile on an exponential erasure process. Assuming that the microscopic erasure process is exponential in nature, then the time dependence of the *local* grating amplitude g(t) satisfies

$$dG(t)/dt = -\alpha G(t)$$

where α is the erasure rate. The erasure of the grating in the fiber, however, is inhomogeneously broadened by the non-uniform intensity profile of the fiber modes. The total induced second harmonic as a function of erasure time is given by the integral of the time-dependent local grating amplitude multiplied by the electric fields involved in generation of second harmonic from the grating

$$E_{SHG}(t) \propto \int_0^{\infty} G(r, t)E_{\omega}^{2}(r)E_{2\omega}^{*}(r)rdr$$

where $G(r,t) = G_0 e^{-\alpha(r)t}$. We assume that the initial grating amplitude G_0 is independent of the transverse coordinate r. Approximating the IR and second-harmonic modes as Gaussian with waist sizes w_1 and w_2:

$$E_\omega(r) = E_{\omega 0} e^{-r^2/w_1^2}$$

$$E_{2\omega}(r) = E_{2\omega 0} e^{-r^2/w_2^2}$$

the erasure rate α is proportional to a power β of the erasure intensity I_e, $\alpha = \alpha_0 I_e^\beta$ then the time-dependent erasure of the second-harmonic field strength is given by

$$E_{SH}(t) \propto \frac{1}{\beta}\int_0^1 u^{[K-1]} e^{-I_e^\beta tu} du \qquad (2)$$

where $K = \dfrac{[1 + w_1^2/2w_2^2]}{w_1^2/\beta w_2^2}$. We show that the time dependence given by the integral in Eq. 2 can be approximated by a power law (Fig. 4). The data points are generated using the Gaussian profile model and are fit with the power law given by Eq. 1. As can be seen from the figure, the approximation is very good. Thus, while the microscopic process may well be exponential, the power law can be explained by taking into account the transverse profile of the beams. We note that other inhomogeneities, such as an energy distribution of defect levels, may also contribute to the power law behavior.

From erasure rate measurements over a range of erasure intensity, we determine the green photon number involved in the erasure process. The photon number β is given by the slope of the erasure rate vs. erasure intensity curve in log-log scale. We find that the photon number determined using the power law is identical to the photon number found with the Gaussian profile model. From our data, the number of green photons involved in erasure is 3.8±0.2 (Fig. 5). This differs from the values expected from a straightforward 2 green photon or 4 fundamental wavelength photon photovoltaic model. Tsai and Griscom[15] explained this four green photon dependence by the bleaching of Ge-associated defect centers, and determined the photon number about four.

Our possible explanation is based on the experimental evidence from Carvalho et al.[14] that a metastable intermediate state exists in the grating formation process responsible for SHG in optical fibers. The physical picture is shown in Fig. 6 Between the

ground and the ionization state, there is a metastable state with decay constant γ. The rate equations can be written a

$$\dot{\rho}_1 = -\alpha\rho_1$$
$$\dot{\rho}_2 = \alpha\rho_1 - \beta\rho_2 - \gamma\rho_2$$
$$\dot{\rho}_3 = \beta\rho_2$$

Where α, β are the excitation coefficients from ground state and metastable state respectively, γ is the decay coefficient for the metastable state, ρ_1, ρ_2 and ρ_3 are the electron densities at the ground, metastable, and ionization states respectively.

At steady state, $\dot{\rho}_2 = 0$. If we assume that $\alpha = aI_{2w}^2$, $\beta = bI_{2w}^2$ for two photon absorption between levels, where a and b are constants, then we obtain the ionization rate

$$\dot{\rho}_3 = ab\rho_1 I_{2\omega}^4/(bI_{2\omega}^2 + \gamma)$$

We consider the limiting cases. When $bI_{2w}^2 >> \gamma$, the metastable state is saturated and $\dot{\rho}_3 \approx \rho_1 aI_{2\omega}^2$ When $bI_{2w}^2 << \gamma$, we get a different power dependence $\dot{\rho}_3 \approx \rho_1 abI_{2\omega}^4/\gamma$. If we assume the erasure rate is proportional to the ionization rate, then this model gives the erasure rate proportional to the second to fourth power of the erasure intensity, depending on whether the metastable state is saturated or not. Our green erasure rate proportional to the (3.8±0.2)th power of erasure intensity (Fig. 5) lies within this power dependence range and is closer to the lower erasure intensity end. But we could not go to lower erasure intensities due to noise and the fact that it would take many many hours to erase the grating. It is also hard to reach higher erasure intensities because of the damage threshold of the fibers.

Conclusion

Seeded $\chi^{(2)}$ grating growth/green-light erasure is reversible. The non-exponential time dependence can be explained by inhomogeneous broadening due to the intensity profile of the fiber modes. The photon number of the erasure process is 3.8±0.2. A possible explanation of the photon number is based on the existence of an intermediate excited state.

Acknowledgments

The authors wish to thank Dr. Boris Ya. Zel'dovich for very helpful and stimulating discussions and to thank John Weiss for assistance in the experiment.

Figure Captions

Fig. 1 Experimental setup. A is an attenuator, F is a colored glass filter, PA is a phase adjuster, BS is a beamsplitter, HBS is a harmonic beamsplitter used to either separate or recombine the IR and SH beams, KTP and KDP are frequency-doubling crystals.

Fig. 2 The reversibility test. The $\chi^{(2)}$ grating seeded growth/green-light erasure process is reversible. This sample curve shows 10 cycles of growth and erasure in a single fiber.

Fig. 3 A typical time dependent $\chi^{(2)}$ grating green-light erasure curve with a power law fit.

Fig.4 A power law fit to simulated data. The data points are generated from the Gaussian profile model(Eq. 2) using a fixed photon number and erasure intensity. We fit the data with a power law(Eq. 1).

Fig. 5 Photon number dependence. We assume that the erasure rate is proportional to a power of the erasure intensity. The slope of the erasure rate vs. erasure intensity curve in log-log scale gives a photon number of 3.8±0.2.

Fig. 6 The physical picture of the energy levels involved in the grating formation/erasure process, including a metastable intermediate state with decay constant γ.

References

[1] U. Osterberg and W. Margulis, Opt. Lett., 11, 516, 1986.

[2] U. Osterberg and W. Margulis, Opt. Lett., 12. 57, 1987.

[3] R. H. Stolen and H. W. K. Tom, Opt. Lett., 12, 585, 1987.

[4] M. C. Farries, P. St. J. Russell, M. E. Fermann, and D. N. Payne, Electron. Lett., 23, 322, 1987.

[5] N. M. Lawandy, Phys. Rev. Lett., 65, 1745, 1990.

[6] D. Z. Anderson, V. Mizrahi, and J. Sipe, Opt. Lett., 16, 796, 1991.

[7] F. Ouellette, K. O. Hill, and D. C. Johnson, Opt. Lett., 13, 515, 1988.

[8] A. Krotkus and W. Margulis, Appl. Phys. Lett., 52, 1942, 1988.

[9] B. Ya. Zel'dovich and Yu. E. Kapitskii, Sov. J. Quant. Electron., 20, 869, 1990.

[10] B. Ya. Zel'dovich, Yu. E. Kapitskii, and V. M. Churikov, JETP Lett., 53, 79, 1991.

[11] Y. Hibino, V. Mizrahi, and G. I. Stegeman, Appl. Phys. Lett., 57, 656, 1990.

[12] I. C. S. Carvalho, W. Margulis, and B. Lesche, Electron. Lett., 27, 1497, 1991.

[13] B. Ehrlich-Holl, D. M. Krol, R. H. Stolen, and H. W. K. Tom, Opt. Lett., 17, 396, 1992.

[14] I. C. S. Carvalho, W. Margulis, and B. Lesche, Opt. Lett., 16, 1487, 1991.

[15] T. E. Tsai and D. L. Griscom, International Workshop on Photoinduced Self-organization Effects in Optical Fibers, Francois Ouellette, Ed., Proc. SPIE 1516, 14, 1992.

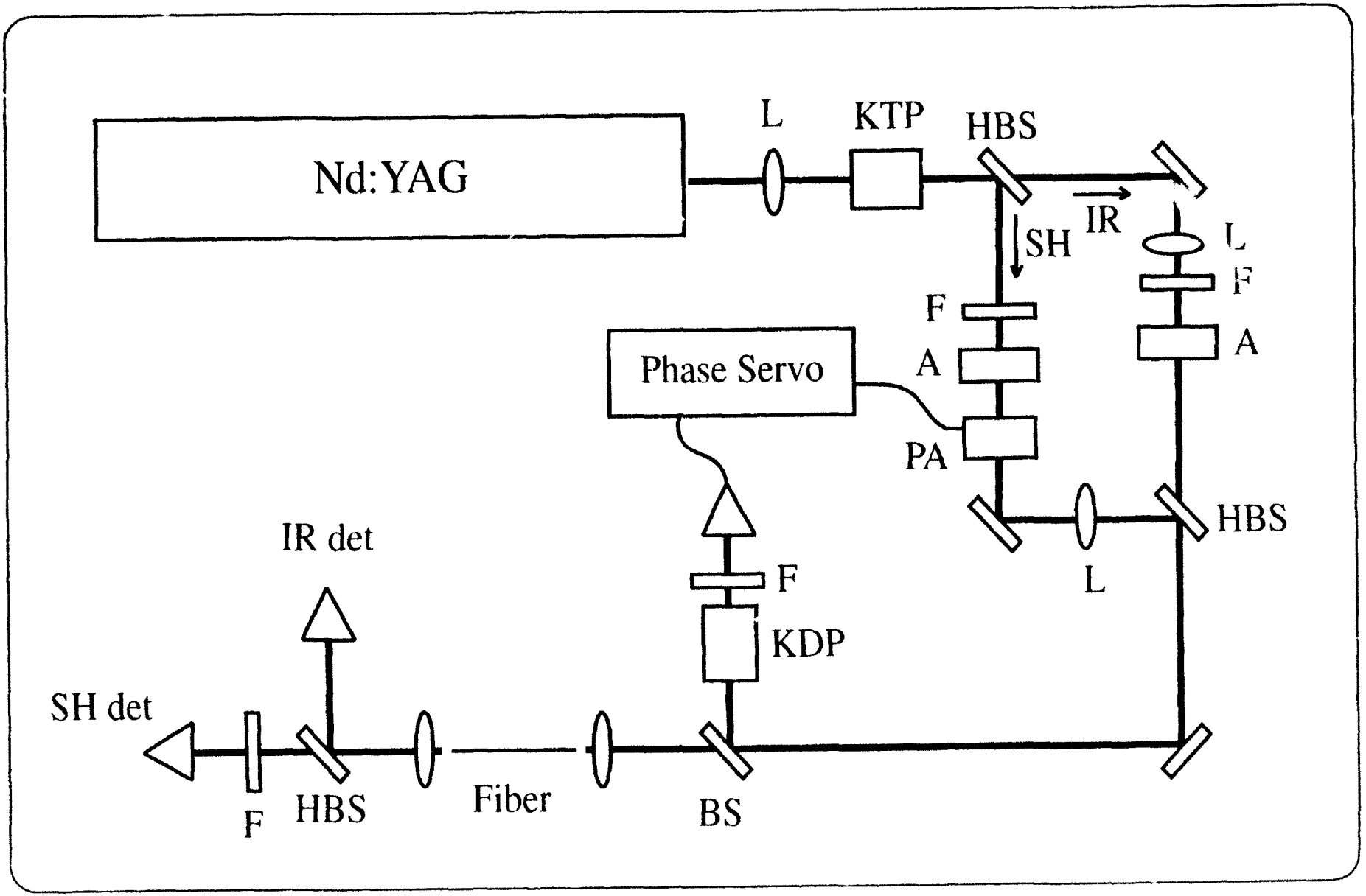
Nd:YAG
L
KTP
HBS
IR
SH
L
F
A
F
A
Phase Servo
PA
HBS
L
IR det
F
KDP
SH det
F
HBS
Fiber
BS

Fig 1

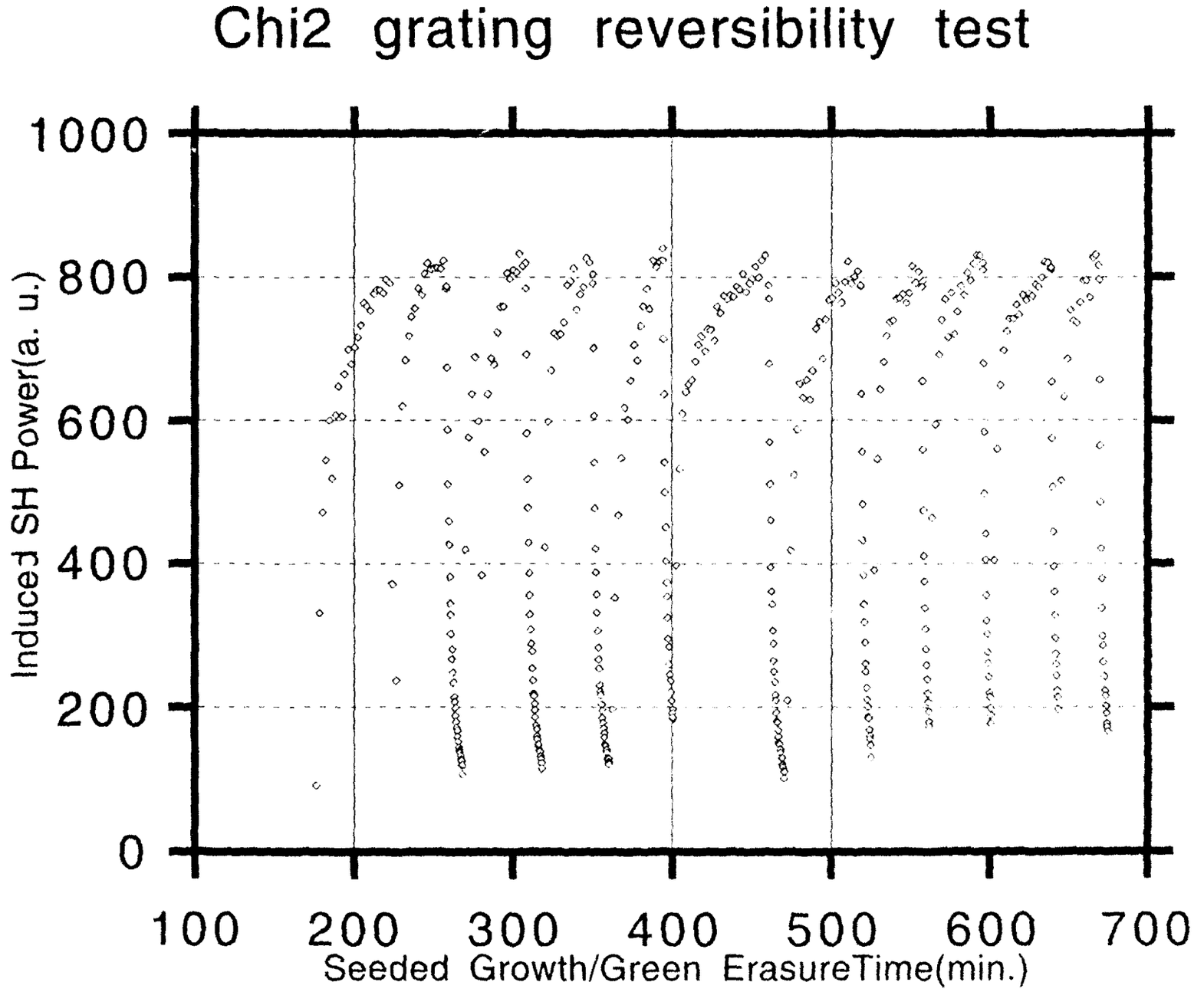
Chi2 grating reversibility test
Induced SH Power(a. u.)
1000
800
600
400
200
0
100
200
300
400
500
600
700
Seeded Growth/Green ErasureTime(min.)

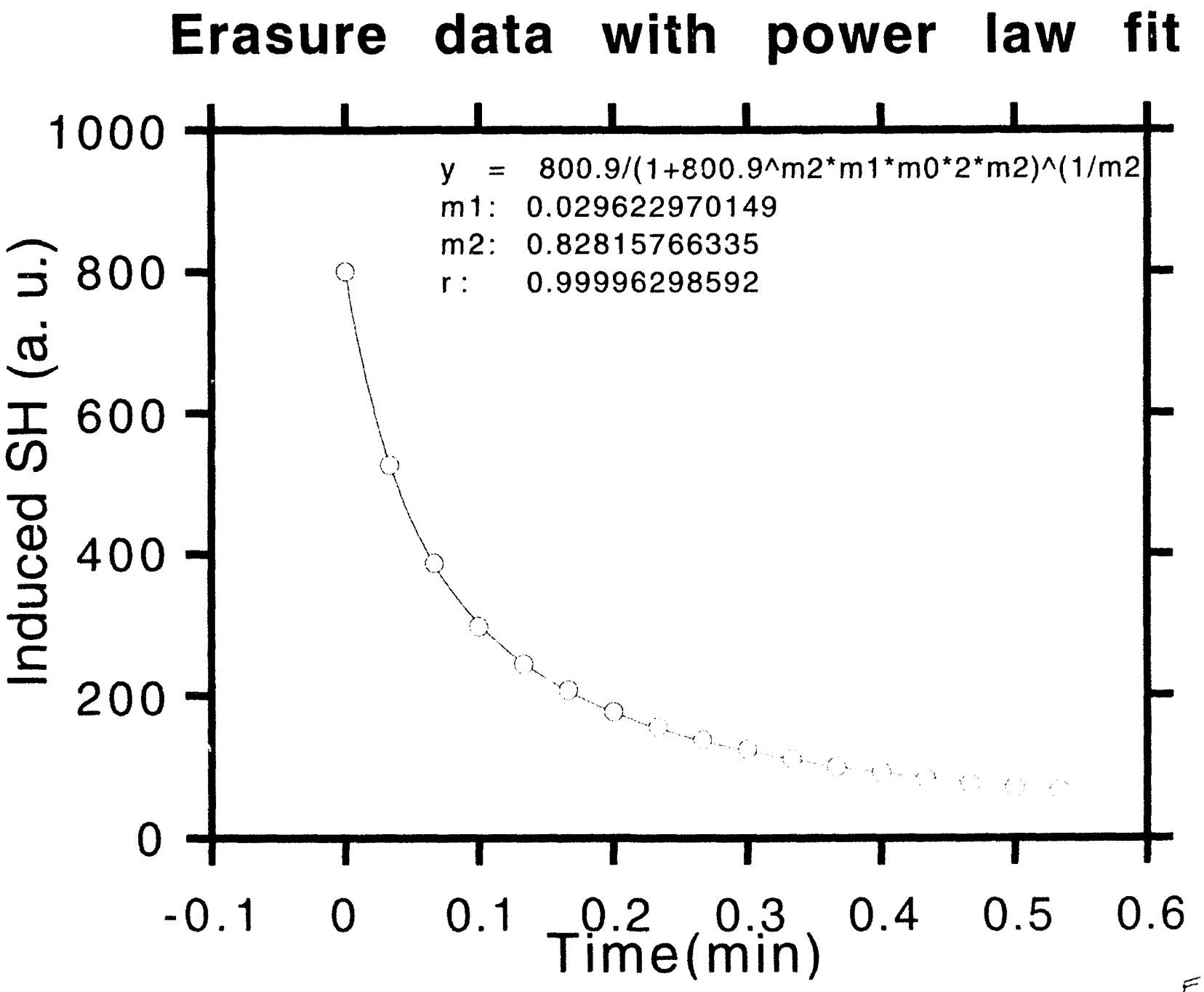
Erasure data with power law fit
y = 800.9/(1+800.9^m2*m1*m0*2*m2)^(1/m2
m1: 0.029622970149
m2: 0.82815766335
r: 0.99996298592
Induced SH (a. u.)
1000
800
600
400
200
0
-0.1
0
0.1
0.2
0.3
0.4
0.5
0.6
Time(min)

Fig 3

Fit of generated erasure data with power law

(I = 1; Beta = 3; Wrat = 2)

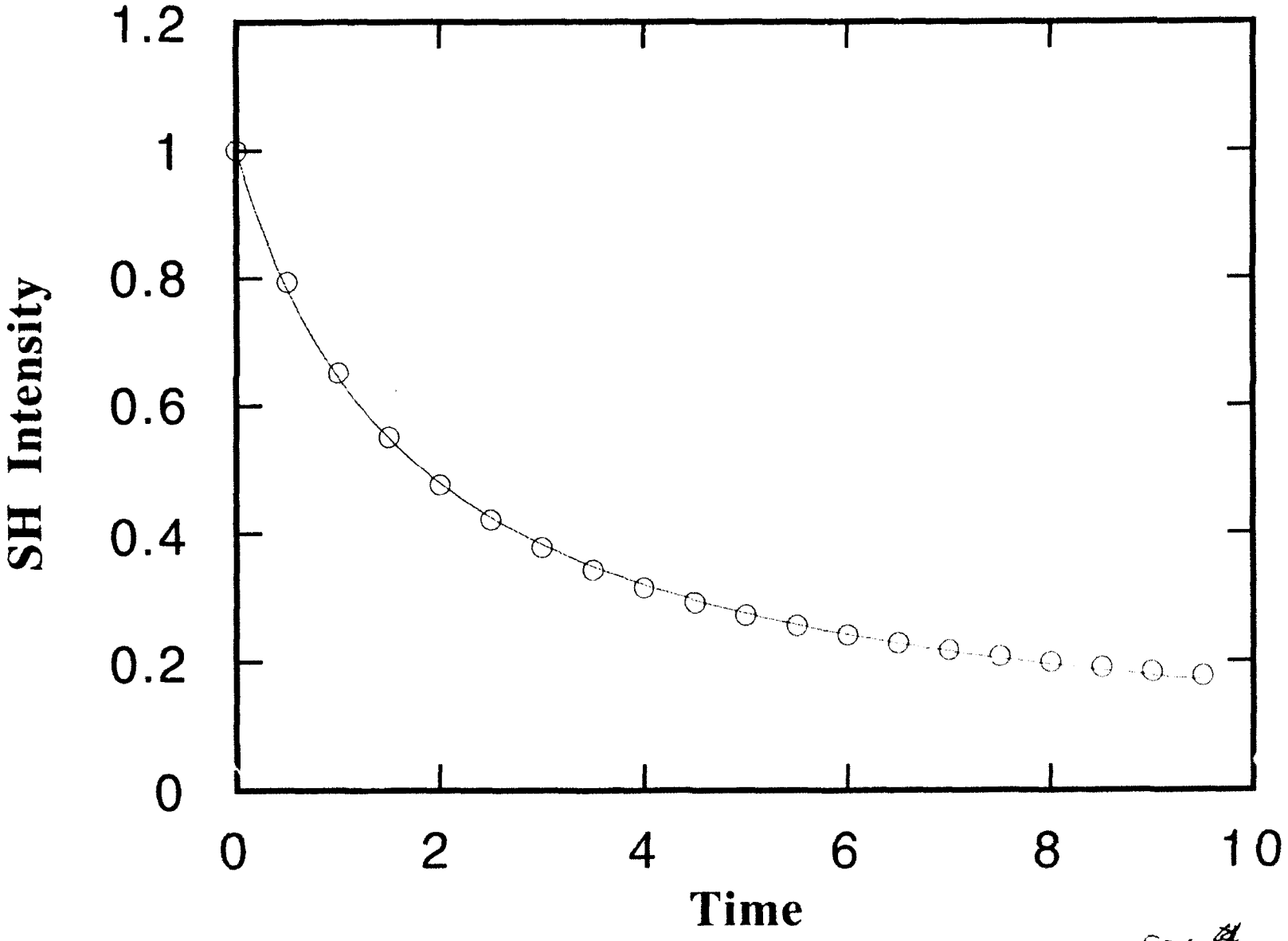

FIG 4

Erasure rate vs. erasure intensity curve

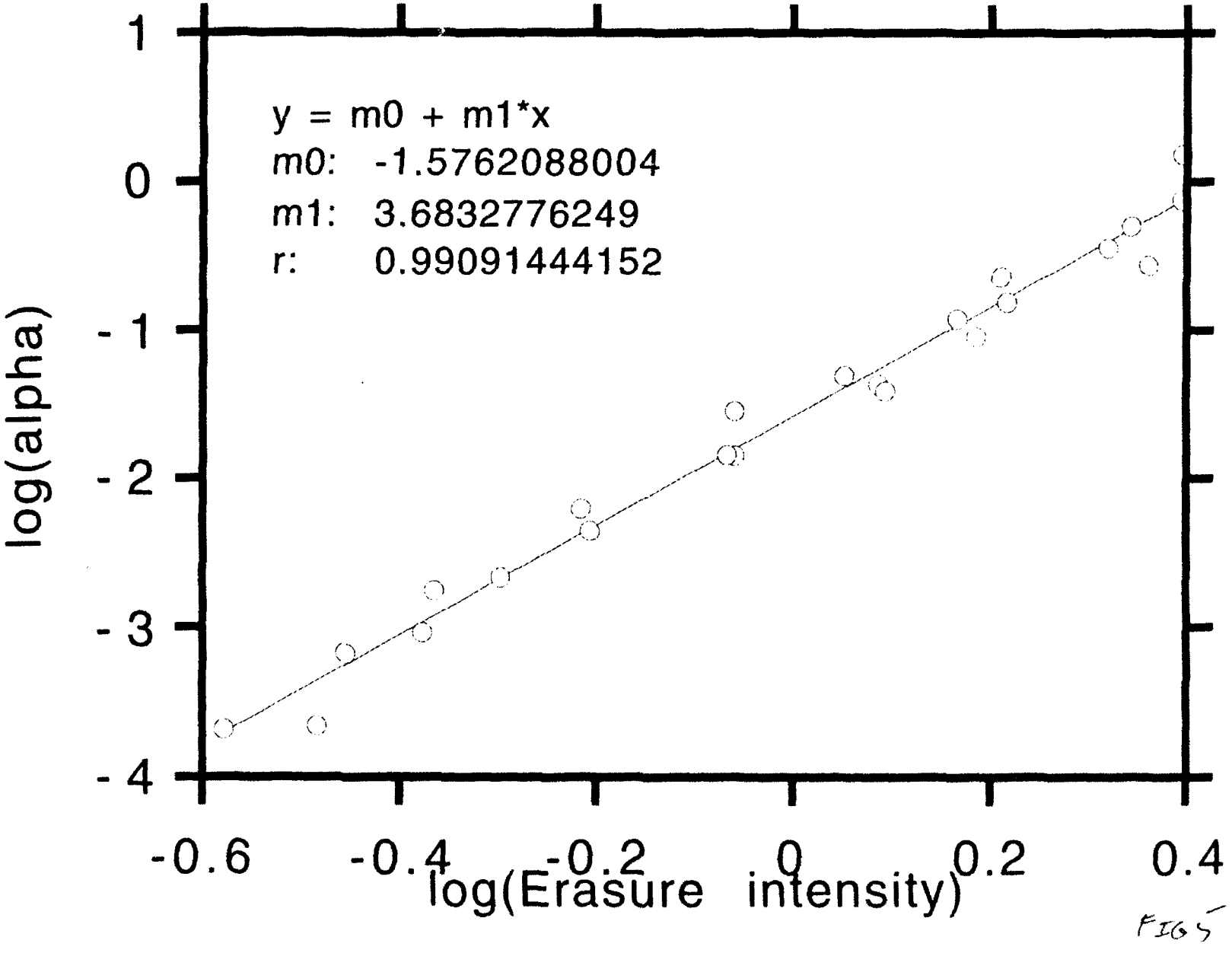

FIG 5

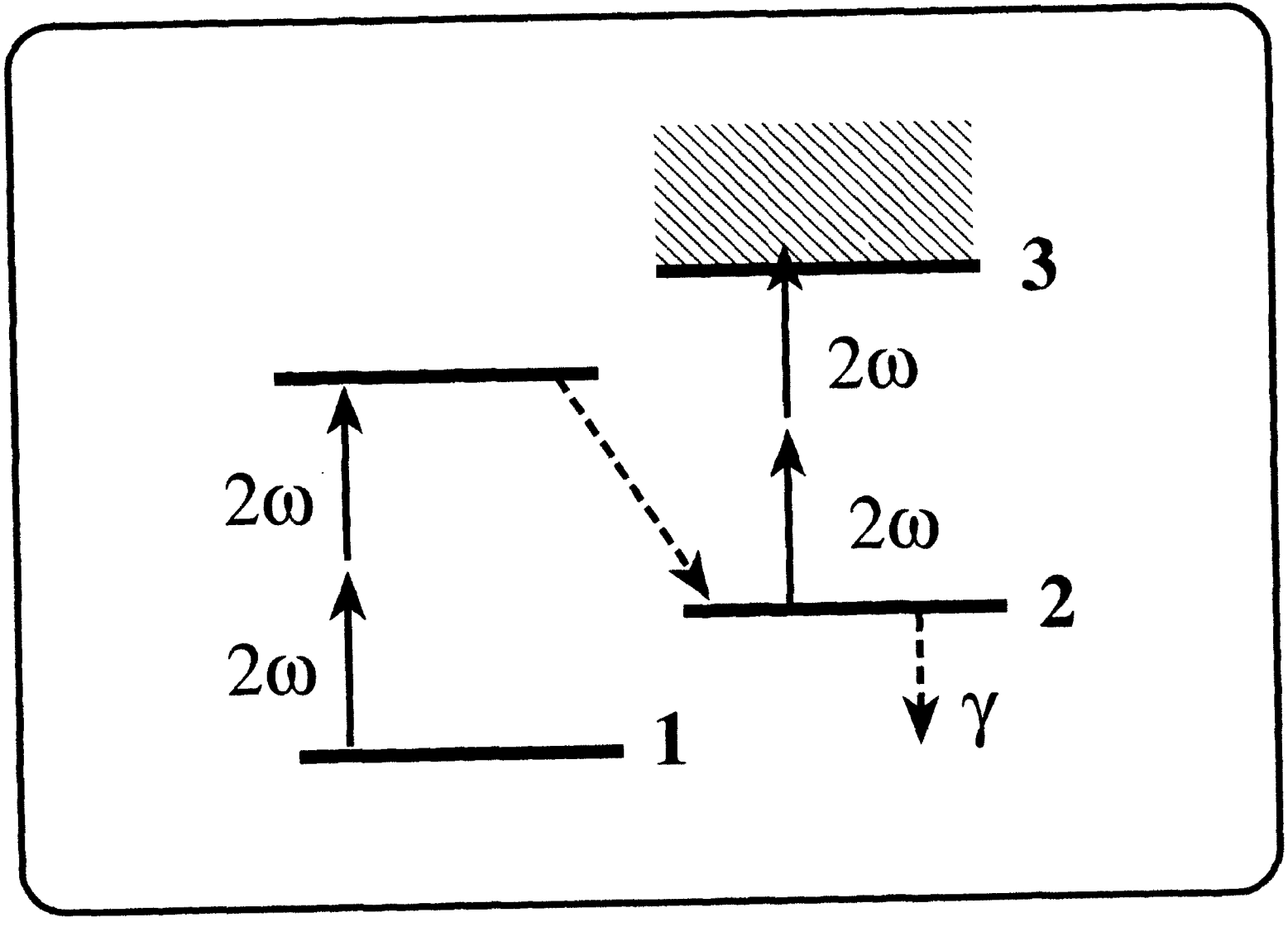

FIG 6

A Final Report on AFOSR Contract #AFOSR 90-0198

APPLICATIONS OF THE PHOTOREFRACTIVE EFFECT AND DAMAGE INDUCED EFFECTS IN FIBERS

Submitted to

THE AIR FORCE OFFICE OF SCIENTIFIC RESEARCH

by

Dana Z. Anderson
Department of Physics and Joint Institute for Laboratory Astrophysics
University of Colorado, Boulder, CO 80309-0440

APPLICATIONS OF THE PHOTOREFRACTIVE EFFECT AND DAMAGE INDUCED EFFECTS IN FIBERS

I. INTRODUCTION

This is a final report of work carried out under AFOSR contract #AFOSR 90-0198. The focus is two-fold. One aspect concerns photoinduced effects in fibers, especially the processes of self-organized second-harmonic generation in fibers. For the most part we have developed the microscopic theory of second-harmonic generation in fibers as far as possible in absence of a micro and mesoscopic theory of defect formation in glass. The basic physics involved in second-harmonic generation in fibers has led to a number of other possible experiments and applications. For example, it is known that a photogenerated current cannot be produced by a single optical beam illuminating a centrosymmetric medium but it is now recognized that a current can be generated in a centrosymmetric medium by illumination with two harmonically related optical fields. However, we have concluded that as an *application*, self-organized second-harmonic generation in fibers does not appear to be a practical means of frequency doubling conventional lasers. Thus, until a conceptual or practical breakthrough occurs, we have brought to a close the experimental and theoretical work on this subject.

The second aspect concerns the dynamics and self-organization of photorefractive optical circuits. In past work we have produced circuits that self-organize according to the nature of their time dependent input. After self-organizing they process information in an adaptive and useful way. Our most highly developed circuit in the previous report was a demultiplexer that separates signals from a multimode fiber. In this past year we analyzed and began construction of an optical system that is to implement what is known as a self-organizing topology preserving Kohonen map [1]. Kohonen maps learn about the topological properties of their input environment, and provide a powerful means to process data such as images, especially data where *a priori* little is known about the topological relationship of the input data at various times. Kohonen networks have been used successfully, for example, to process acoustic signals (including speech) and in solving various optimization problems such as the traveling salesman problem. The dynamics of a Kohonen network are natural to the nonlinear photorefractive systems that we have previously developed. The work involves characterizing the spatio-temporal dynamics of photorefractive systems. In so doing we have formulated the theory of transverse instabilities of a single photorefractive coupling and outlined the analogies and differences with those observed in Kerr media [2, 3, 4]. In particular we looked at the formation of hexagonal patterns [5, 6, 7].

The bulk of the theoretical and experimental work on second harmonic generation is collected in the thesis of Dr. James Leitch, and the work on the reversibility and time-dependence of the $\chi^{(2)}$ gratings responsible for second-harmonic gratings are included in a preprint which we include with this report. The remainder of this report gives a detailed account of the work on self-organization and dynamics in photorefractive systems. The following section gives a brief overview of Kohonen Networks. Section III discusses the preliminary optical implementation as well as some of the experimental results. In particular, we find the optical system exhibits an interesting instability which we have analyzed and found to be caused by the finite and inevitable misalignment of the optical system. We discuss the "wandering spot" behavior in Section IV. The investigation of dynamics led to a tangential but related theoretical investigation of spatial instabilities in pumped photorefractive media. This investigation is presented in section V. We wrap up the report with a discussion of numerical modeling of optical Kohonen maps and discuss prospects for future work in section VI.

II. KOHONEN TOPOLOGY PRESERVING MAPS

The schematic drawing of a Kohonen topology preserving map is shown in Fig. 1, drawn using what is by now conventional neural network symbols. The key element in the network is a layer of mutually interacting nonlinear elements, and a collection of weights that connect each input element to the input of every nonlinear processing element. The weight, or connection strengths of each of the line from input to processing unit determines the extent a given input communicates with a given processing element. A given collection of input stimulates the processing units, and the latter units want to "turn on" However, they are competitive, so that one unit turning on causes the others to be turned off, more or less. The competitive interaction in steady state is such that only one output, or a localized collection of outputs, are on, the others are forced off. This is called winner-takes-all (WTA) behavior. The winning unit (or collection)

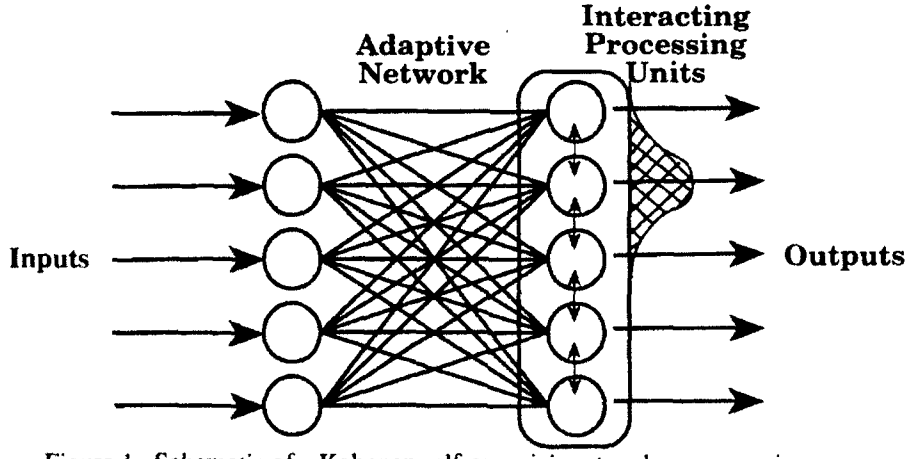

Figure 1. Schematic of a Kohonen self-organizing, topology preserving map.

adjust their connection weights to the input in such a way that the next time the very same input appears, it is all the more likely that the same units again win the competitive interaction. This WTA competition and subsequent weight updating takes place for each of many inputs.

This seemingly simple set of processing sequences gives rise to surprisingly powerful processing capability [1]. in steady state, the response of the outputs will reflect the topological organization of the input space. That is topologically nearby inputs will excite neighboring output. In another view, if say the inputs are a collection of images, the network will discover what images are more similar or more dissimilar so that similar images will excite neighboring outputs, dissimilar inputs will excite more distant outputs. The more distant the inputs, the more distant the outputs.

The essential ingredients of the Kohonen network are a) the adaptive interconnections from the input to the processing units and b)the WTA interaction among output units.

III. Optical Kohonen Network

We have implemented the essential features of the Kohonen network using a simple two-photorefractive crystal optical system, illustrated in Fig. 2.. The figure also establishes a rough analogy between the Kohonen network drawn above and the optical system. The major anological difference being that the output processing elements as well as the interconnections are essentially a continuum, instead of a discrete set.

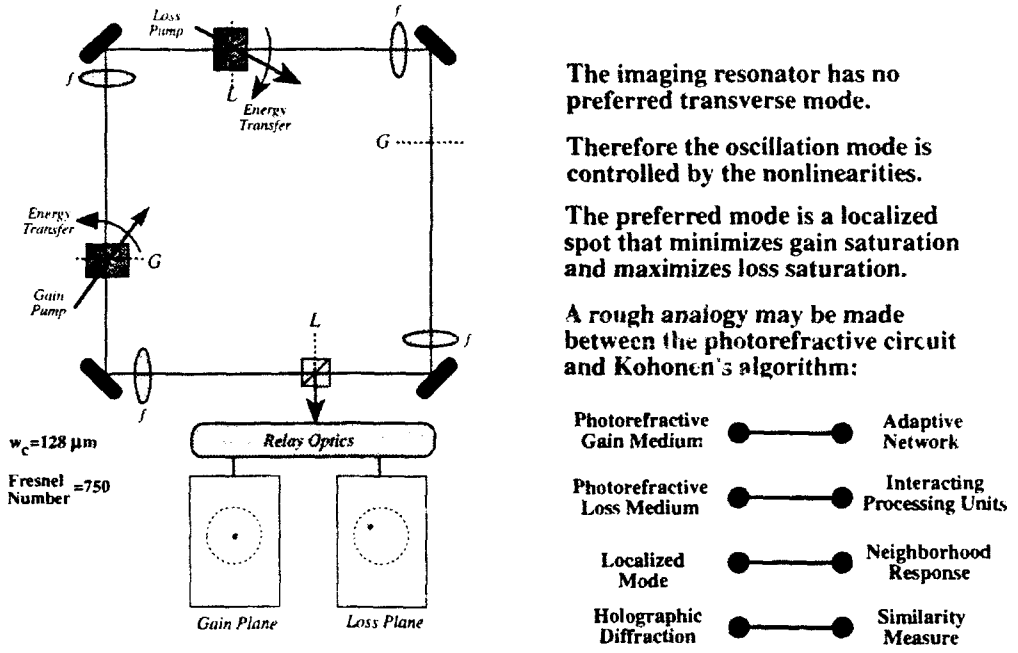

Figure 2. Imaging resonator for Kohonen self-organizing map implementation.

The optical circuit is composed of an imaging resonator with a photorefractive gain medium and a photorefractive loss medium. The two media are in conjugate planes, that is, the loss medium lies in the Fourier plane of the gain medium, and vice versa. The gain medium serves also as the interconnection weights. Input data is provided by placing images, or other information on the gain pump laser beam.

Our recent work has primarily focused on the complex dynamics of the system in Fig. 2. If we consider for a moment a static pump (no information imposed on it) we can qualitatively describe the winner-takes all behavior: An imaging resonator has no well defined modes (or an infinite set of modes). Thus, practically any self-consistent field distribution can oscillate in the ring resonator given sufficient gain. In order to optimize the energy available from the pump laser, an oscillating field tries to match the size of the pump beam, which is chosen to be relatively large. On the other hand, the loss medium modifies the oscillation characteristics. The photorefractive loss medium behaves somewhat like a saturating dye absorber, except that in our case the saturating intensity is directly determined by the loss pump intensity. The oscillating field most effectively minimizes its loss by becoming as small as possible, because, for the same amount of total power it can best reach the saturation intensity. Because the gain and loss are in conjugate optical planes, these two energy maximization strategies in the gain and loss medium complement each other. A large beam in the gain medium corresponds to a small one in the loss medium. On the other hand, there is no preferred location in the loss medium provided the loss pump has a uniform intensity. Therefore, *the oscillation in the ring will form a small spot,*

anywhere in the loss plane. This corresponds to a winner-takes-all behavior in a two-dimensional spatial continuum.

With the loss pump not present, the oscillator has no preference for a small spot in the (would-be) loss plane, so a very broad oscillating field arises. Fig. 3 shows the experimental results of the collapse of the transverse mode profile of the oscillating beam as the loss pump is first allowed to induce loss in the resonator. Shown are the oscillation intensities in both the loss and the gain planes. Note the collapse of the oscillation in the loss plane from a broad oscillating distribution to a single small spot. The image of the gain plane also appears to show some reduction in spot size but in fact the spot is merely decreasing its overall intensity in response to the additional net loss in the ring resonator.

IV. Wandering Excitations in a Photorefractive Ring Resonator

While the imaging gain and loss resonator did exhibit winner-takes-all behavior, we found that the output spot position in the loss plane was spatially unstable [8]. We have spent considerably effort developing an appropriate model for this instability. In this section we discuss the experimental and theoretical investigation of this phenomenon.

The eigenmodes of a linear or nonlinear oscillator are found by imposing self consistent boundary conditions such that the oscillator field is equal to itself after one round trip of propagation. The field eigenmodes found in this way normally correspond to stationary distributions of the electric field. In some special cases no such stationary solutions exist. In this case the eigenmodes describe an electric field profile which continuously changes in time. A clear distinction may be made between this situation and that of an unstable multimode resonator, within which the electric field profile continuously changes due to the excitation of one or another stationary transverse mode, or the simultaneous excitation of multiple modes, each with a distinct eigenfrequency.

The near imaging ring resonator with photorefractive gain and loss is an example of an oscillator with nonstationary eigenmodes. We redraw the schematic here in Figure 4 to illustrate the experimental and numerical investigation of the spatial instability mentioned in the previous section.

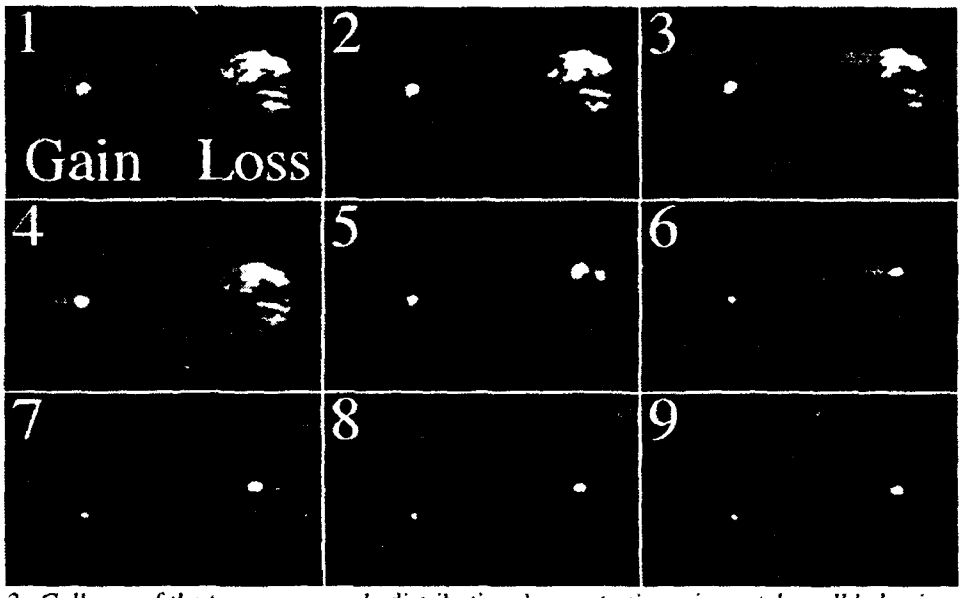

Figure 3. Collapse of the transverse mode distribution demonstrating winner-takes-all behavior of the imaging resonator with gain and loss. The pictures correspond to 1/30 of a second between video frames.

In the single transverse mode ring oscillator with photorefractive gain and loss the nonlinearities lead to bistability and self-pulsing [9, 10]. In the imaging ring with gain and loss the nonlinearities interact in a different manner, leading to spatial mode collapse as described above. In the imaging ring resonator [11] any transverse field profile is imaged onto itself after one cavity round trip, thus the empty resonator supports a continuum of transverse modes.

Since the linear cavity has no influence on the field profile the effect of the photorefractive nonlinearities assumes added importance. To give the example in the previous section a more concrete form, suppose the oscillation mode can be approximated by a Gaussian. Then its Fourier transform is also a Gaussian with a width inversely proportional to the input Gaussian. Place a photorefractive saturable gain nonlinearity, which tends to broaden a Gaussian profile, in one plane, and the complementary photorefractive saturable loss nonlinearity, which tends to narrow a Gaussian profile, in the conjugate plane. Thus both nonlinearities cooperate to encourage the formation of a narrow Gaussian in the plane of the loss medium.

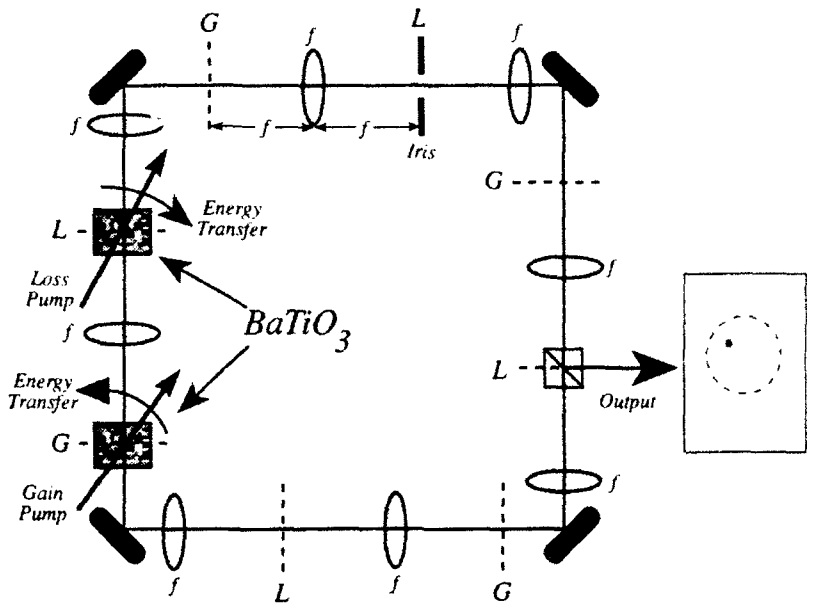

Figure 4. Imaging ring resonator with photorefractive gain and loss. All lenses are f=100 mm with a spacing of 2f. The gain and loss pumps are from a cw Argon laser, λ=514 nm.

However, as indicated above, the experimental realization of this device showed that the localized field excitation drifts in the transverse plane of the resonator [8]. An example of this motion is shown in Fig. 5. The excitation appears at some point in the aperture and then drifts in a direction determined by the cavity alignment.

Depending on the details of the cavity alignment, and the gain and loss pump intensities, the spot either drifts to the edge of the aperture and disappears before reappearing again in its original position, or else it executes a cyclic motion wholly within the aperture. In the latter case the spot does not move in a closed circle but rather appears, moves a short distance, and then disappears, before repeating its motion. It takes a few seconds for the spot to execute a single traverse across the aperture. The spot will typically choose a new drift path after about 10 cycles along any given path.

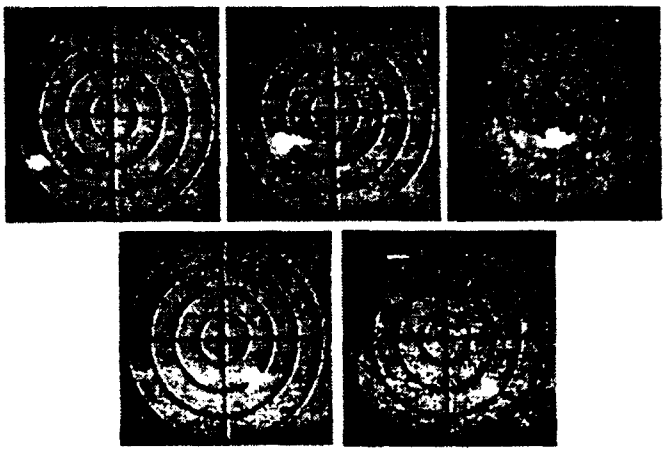

Figure 5. Experimental observation of spot motion. Frames were recorded at 0, 3, 7, 9 and 10 seconds of elapsed time in pictures from left to right, top to bottom.

The wandering motion, alternating between paths that are each repeated a few times, continues indefinitely. The spot motion appears to be determined by the cavity alignment since small adjustments to one of the resonator mirrors change the spot trajectory noticeably.

The spot motion has been simulated by numerical calculations of the resonator dynamics. The optical field and the photorefractive gratings are discretized on a square lattice. We assume no crossing of the pump and signal beams in the gain or loss crystals, but retain the axial dependence of the field and gratings in each crystal. Thus there is no interpixel coupling within the crystals. The transverse coupling which leads to mode collapse arises from placing the crystals in spatially conjugate planes. If the cavity is assumed to be perfectly aligned the spot forms in a location determined by the maximum of the initial seeding, and is stationary. Misalignment of the cavity is modeled by introducing a phase wedge in the cavity $\Phi(x,y) = \exp i\left(\delta_x x + \delta_y y\right)$, where x, y are the transverse coordinates and δ_x, δ_y characterize the slope of the wedge. Placing the wedge next to the gain crystal results in a continuous motion of the spot parallel to the wedge gradient $\bar{\nabla}\Phi \sim \delta_x \hat{x} + \delta_y \hat{y}$. An example of numerical simulations using 21 x 21 grid points is shown in Fig. 3. for $\delta_x/\delta_y = 2$ and $\delta_x x_{aperr} = 1$, where x_{aperr} is the total width of the aperture in Fig. 3. Additional calculations indicate that the rate of spot motion is proportional to δ for small δ. The observed trajectory shown in Fig. 2 does not lie on a straight line because the cavity misalignments are not well characterized by a simple linear wedge.

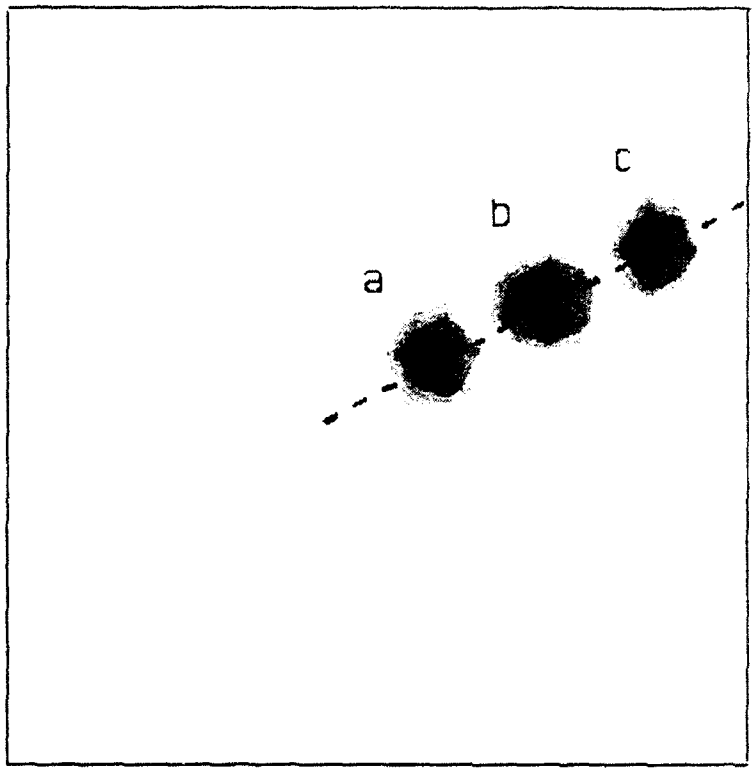

Figure 5. Calculated spot motion. The excitations labeled a,b and c correspond to 400, 1800 and 3000 gain crystal time constants. The dashed line is drawn parallel to $\vec{\nabla}\Phi$.

In conclusion we have shown that the oscillation pattern in a near imaging ring resonator with photorefractive gain and loss is localized but does not have a well defined position. Numerical simulations show that the motion of the field excitation is governed by small misalignments of the optical cavity.

V. TRANSVERSE INSTABILITY OF COUNTER-PROPAGATING WAVES IN PHOTOREFRACTIVE MEDIA

The desire to understand the dynamics of the imaging resonator also led us to consider simpler photorefractive instabilities. Small-scale transverse instability of a single beam or two counter-propagating beams in a Kerr-type nonlinear medium has been known in nonlinear optics for some time (see e.g. [2, 3, 4]). The instability manifests itself by the generation of a pair of satellite beams traveling at small angles $\pm\theta_c$ to the primary beams. The interference of the primary and satellite beams results in a transverse intensity modulation with the characteristic spatial scale $l_s = 2\pi/\theta_c k_0$. This transverse modulation is now attracting attention in connection with the formation of patterns in nonlinear optical systems [5, 6]. In the case of counter-propagating beams the nonlinear stage of the instability may, in some cases, result in the formation of hexagonal or square patterns with the size of the patterns being determined by the

characteristic spatial scale l_s of the linear stage. Up to now patterns have been observed in atomic vapors [7] and liquid crystals [12]. It has been suggested [13] that photorefractive crystals may be a suitable choice for nonlinear medium since they exhibit high nonlinearities and the value of nonlinear coupling in the crystal can be easily varied by external means. However, important differences between the Kerr and photorefractive nonlinearities warrant the separate analysis of transverse instabilities of counter-propagating beams that is presented here.

For the case of a single beam propagating through a nonlinear medium the onset of the convective instability corresponds to the appearance of intensity modulation on its transverse profile with the characteristic modulation period considerably less than the diameter of the beam. Instability is possible for a range of angles θ between the wavevector $\bar{k}_0$ of the strong plane wave F_0 and the wave vectors $\bar{k}_{\pm 1}$ of the sidebands $F_{\pm 1}$, (Fig.6a). The characteristic angle, corresponding to the largest amplification, is given by the condition $\theta_c^2 \propto n_2 |F_0|^2$, where n_2 is the Kerr coefficient of the medium.

Similarly two strong plane waves F_0 and B_0 counter-propagating in a Kerr medium turn out to be unstable versus excitation of two pairs of waves: $F_{\pm 1}$ and $B_{\pm 1}$ situated as shown in Fig.6b [4]. An important difference in the case of counter-propagating beams is that the system is now absolutely unstable.

The general nature of the transverse instability is preserved in photorefractive media, although not the details of the instability threshold conditions. This is due to several differences between the photorefractive and Kerr-type nonlinearities. In Kerr-type media the nonlinear part of the refractive index n_2 is not (or is only weakly) dependent on the angle θ between the interacting waves (see Fig.6) or, equivalently, on the wavevector $k_\perp = \theta k_0$ of the grating written by the pumping waves with their sidebands (F_0 with $F_{\pm 1}$ and B_0 with $B_{\pm 1}$) and so the characteristic angle θ_c is the result of interplay between the Kerr nonlinearity and diffraction. The nonlinear coupling coefficient (analog of n_2) in photorefractive media is strongly dependent on the value of $k_\perp$ and so material properties of the crystal must come into play, imposing their

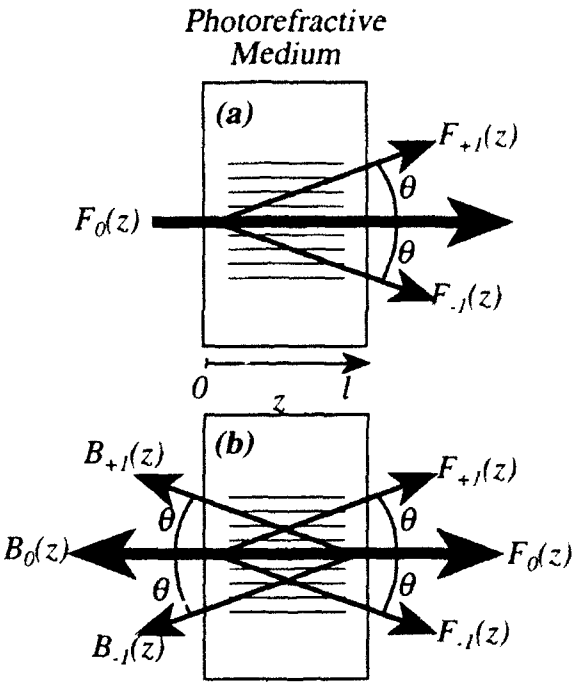

Figure 6. Geometry of the optical interaction. a) Excitation of satellite beams by a single primary beam. b) Excitation of pairs of satellite beams by counter-propagating primary beams.

own characteristic spatial scales. Furthermore, the Kerr nonlinearity corresponds to a nonlinear change of phase (n_2 is purely real) whereas the photorefractive nonlinearity is in general complex corresponding to both amplitude and phase changes. The magnitude of the real part of the coupling coefficient can be enhanced by applying an external electric field to the photorefractive crystal, but in general it is impossible to completely eliminate the imaginary part. Also the dependence of the real and imaginary parts on the value of $k_\perp$ is different. In addition photorefractive media are characterized by strong amplified incoherent scattering (fanning) which leads to a dependence of the amplitudes of the primary beams on the axial coordinate, even in the linear stage of the instability.

Consider two strong plane waves $F_0 \exp(ik_0 z - i\omega_0 t)$ and $B_0 \exp(-ik_0 z - i\omega_0 t)$ counter-propagating in a nonlinear medium. We will assume that these waves don't interact directly with each other, i.e. the nonlinear medium doesn't support reflection gratings. Let's add a small probe wave $\delta F_1 \exp(ik_0 z + i\vec{k}_\perp \vec{r}_\perp - i(\omega_0 + \Omega)t)$ ($|\vec{k}_\perp| << k_0$, $|\Omega| << \omega_0$) to this system. Interaction of the strong wave F_0 with this probe results in a nonlinear change in the refractive index of the medium proportional to $F_0 \delta F_1^* \exp(-i\vec{k}_\perp \vec{r}_\perp + i\Omega^* t)$ plus its complex conjugate. The conjugate part supports δF_1 whereas scattering of wave F_1 off the first part produces sideband wave

$\delta F_{-1}\exp(ik_0 z - i\vec{k}_\perp \vec{r}_\perp - i(\omega_0 - \Omega^*)t)$. Similarly scattering of wave B_0 off the grating results in the appearance of waves $\delta B_{\pm 1}$ (see Fig.1.b)

Evolution of the satellite beams in photorefractive media is governed by the equations:

$$\begin{aligned}
&(\partial_z + ik_d)F_{+1} = i\tilde{\gamma}_{NL}\left[F_{+1} + F_{-1}^* + q(B_{+1} + B_{-1}^*)\right],\\
&(\partial_z - ik_d)F_{-1}^* = -i\tilde{\gamma}_{NL}\left[F_{+1} + F_{-1}^* + q(B_{+1} + B_{-1}^*)\right],\\
&\\
&(\partial_z - ik_d)B_{+1} = -i\tilde{\gamma}_{NL}\left[F_{+1} + F_{-1}^* + q(B_{+1} + B_{-1}^*)\right],\\
&(\partial_z + ik_d)B_{-1}^* = i\tilde{\gamma}_{NL}\left[F_{+1} + F_{-1}^* + q(B_{+1} + B_{-1}^*)\right],\\
&\tilde{\gamma}_{NL} = \gamma_{NL}/(1+q) \qquad (1)
\end{aligned}$$

with the boundary conditions $F_{\pm 1}(0) = B_{\pm 1}(l) = 0$ corresponding to an absolute instability. Here $q(z) = |B_0(z)/F_0(z)|^2$, $k_d = k_\perp^2/2k_0$ and $\gamma_{NL}(\vec{k}_\perp, \Omega)$ is the complex coupling coefficient, dependent only on material parameters of the medium.

Equations (1) can be solved in closed form for any dependence $F_0(z)$, $B_0(z)$ and any values of q and $\gamma_{NL}(\vec{k}_\perp, \Omega)$ yielding the following dispersion relation for the threshold of the absolute instability:

$$(1 - A_1)(1 - A_2) - A_3 A_4 = 0,$$

$$\begin{aligned}
A_1 &= \beta \int_0^l dz \frac{q(z)}{1+q(z)} \frac{\sin(k_d z)}{\sin(k_d l)} \sinh[s(z-l)],\\
A_2 &= \beta \int_0^l dz \frac{1}{1+q(z)} \frac{\sin[k_d(z-l)]}{\sin(k_d l)} \sinh(sz),\\
A_3 &= \beta \int_0^l dz \frac{q(z)}{1+q(z)} \frac{\sin[k_d(z-l)]}{\sin(k_d l)} \sinh[s(z-l)],
\end{aligned}$$

$$A_4 = \beta \int_0^l dz \frac{1}{1+q(z)} \frac{\sin(k_d z)}{\sin(k_d l)} \sinh(sz),$$

$$\beta = 2\gamma_{NL} k_d / s,$$

$$s = \left[k_d (2\gamma_{NL} - k_d)\right]^{1/2}. \qquad (2)$$

In the case of $q(z) = const$ equation (2) reduces to:

$$\left(q + q^{-1}\right) + \left[(s/k_d)^{-1} - (s/k_d)\right] \sin(k_d l) \sinh(sl) +$$

$$2\cos(k_d l)\cosh(sl) = 0 \qquad (3)$$

Equations (2) or (3) can be solved for s or γ_{NL} as a function of k_d not implying any particular dependence $\gamma_{NL}(k_d)$. They have an infinite number of solutions (branches). In the limiting case of $k_d >> |\gamma_{NL}|$ Eq. (3) gives $i\gamma_{NL} = \pm[-\ln q + i(2N+1)\pi]$ where N is an arbitrary integer. Solutions of Eq.(3) for several low-lying branches are presented in Fig. 6.

Calculations of the photorefractive coupling constant, including its dependence on k_d, [14] indicate that the threshold curves shown in Fig. 6 should be readily attainable in $BaTiO_3$ with modest applied fields of say 100 V/cm, or in $LiNbO_3$ with no applied field. However, such a conclusion would be overly optimistic since we have not yet accounted for the spatial variation of the beam intensities due to optical losses. The intrinsic absorption in photorefractive media is strongly dependent on the impurity doping level. We measured an intrinsic absorption coefficient of $\alpha \sim 2$ cm^{-1} in 0.5 cm thick samples of $BaTiO_3$ and $LiNbO_3$ with what appeared to be average dopant levels. These measurements were made using ordinary polarized beams such that r_{eff} was small and there was only weak generation of fanning. However, a much stronger loss mechanism exists in the light induced broad angle fanning that is characteristic of photorefractive media. Fanning results in very strong depletion of the main beam which can be characterized phenomenologically by an effective absorption coefficient α_f. Measurements in the same sample of $BaTiO_3$ using extraordinary polarized beams which induce strong fanning gave a total effective absorption of $\alpha_T = \alpha + \alpha_f \sim 9\text{cm}^{-1}$, for Gaussian beams of ~ 1 mm diameter.

The quantitative effect of the optical losses on the instability threshold is found by solving Eqs. (4) with $q(z) = q(0)e^{2\alpha_T z}$. and $|F_0(0)|^2 = |B_0(l)|^2$, which minimizes the threshold coupling. The most important feature of the results is that the minimum value of $\gamma_{NL} l$ is now ~9 as compared to ~1.5 without absorption, a value which is still easily accessible in photorefractive

media.

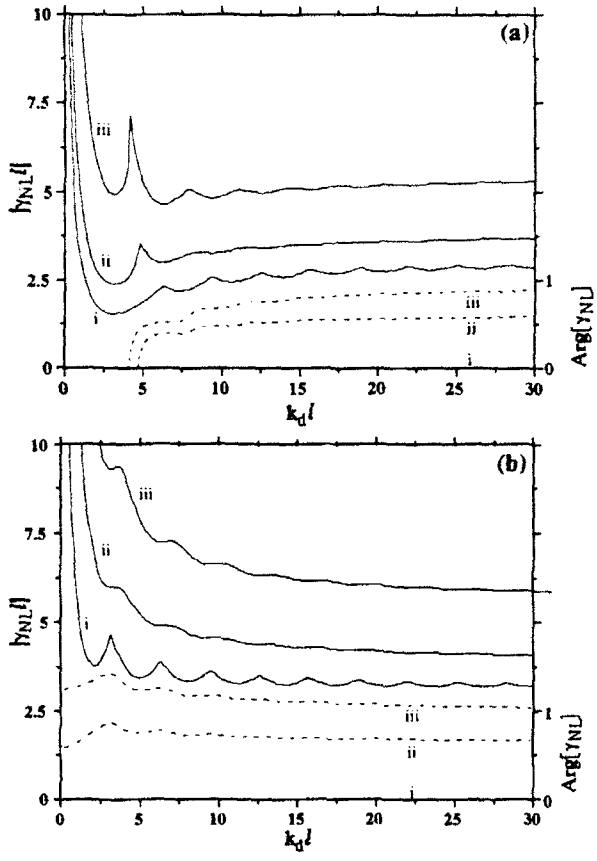

Figure 6. Dispersion curves for q(z)=const.: a) focusing branch with $\mathrm{Re}[\gamma_{NL}] > 0$ and b) defocusing branch with $\mathrm{Re}[\gamma_{NL}] < 0$. The curves are labeled as i) q=1, ii) q=10, and iii) q=100. — $|\gamma_{NL}|$, - - - - $Arg[\gamma_{NL}]$.

Even accounting for optical losses it appears theoretically possible to observe transverse instabilities of counter-propagating beams in photorefractive media. The instability should be accessible with applied fields of several hundred V/cm in $BaTiO_3$ and without applied fields in $LiNbO_3$. Additional calculations, indicate that the threshold should be several times lower still for the same applied field if SBN:75 is substituted for $BaTiO_3$. The reason for the lower threshold in this case is that ε_3 is about 30 times larger in SBN:75 than in $BaTiO_3$ which greatly increases the grating phase shift for the same applied field.

We remain pessimistic as to the likelihood of any such observations in the transmission geometry studied here. The photorefractive coupling coefficients are in principal large enough for the observation of instabilities. Unfortunately, strong photorefractive coupling is intimately connected with strong fanning. The calculations reported here account for fanning losses in the

simplest possible way, as an effective additional absorption. But the effect of fanning may be even more deleterious. The fanning light fills a broad angular region that may mask the otherwise observable instability. In addition, when the fanning is strong, as is the case under conditions favorable for the observation of instabilities, the incident beam acquires a distorted transverse profile, and is no longer well described by a plane wave model. The instability threshold may indeed be many times higher when the beams are strongly distorted.

After completion of this work we became aware of the recent observation of hexagonal patterns due to the formation of reflection gratings in a photorefractive medium [15]. Geometries in which reflection gratings are dominant significantly improve the situation since they allow narrow beams to be employed which greatly reduces the level of fanning. We expect that general features of our results will still be applicable to the reflection geometry, although quantitative predictions of instability thresholds would have to be recalculated. The most significant difference being that the direct coupling between the counter-propagating primary beams leads to a different variation of the beam intensity ratio $q(z)$, than that considered here.

VI. Numerical Simulation of Optical Kohonen Network Behavior

While the experimental and numerical investigation suggest we will need to modify the optical system to be in some way less sensitive to angular misalignments, we can nevertheless demonstrate that the ideal optical system does lead to topology preserving behavior. Using a computer program based upon the work discussed in section IV we simulated a perfectly aligned imaging resonator with data imposed on the gain pump beam. Fig. 7 shows the conceptual schematic of the simulation that follows the experimental work. A laser beam takes on one of four positions in the input plane. The input plane is imaged with a lens into a multimode fiber. The inset marked "input signals" shows the computer simulated image of the beam corresponding to each of the four possible positions.. The multimode fiber completely scrambles the spot location information, so that at the output of the fiber there appears a complex speckle pattern for each of the possible inputs. One such speckle pattern is shown in the figure inset marked "fiber output". The four possible speckle patterns provide the gain pump beam to the imaging resonator. The input beam positions are chosen randomly in time, changing from one spot position to another in times short compared to the response time of the gain medium. In this way, the imaging resonator has seen each possible speckle pattern many times during one time-constant of the gain medium.

The key feature of a Kohonen network is that it discovers the topological relationship among the inputs. In this case the four beam positions are taken from a two-dimensional space and have

the relative relationship in positions shown in the input plane of Fig. 7. Ideally, the output of the optical network would have this same relationship. The measure of distance can change, and a rotation or inversion can take place, but the relative relationships should stay the same. The output plane shown in Fig. 7 represents a correct topology preserving mapping of the input to the output. We note that the resonator output plane inset showing the numerical results is reasonably similar, though not perfectly topology preserving. Despite the imperfection, the simulation demonstrates the remarkable property of the Kohonen mapping that has recognized the topological structure from a very complicated collection of speckle patterns.

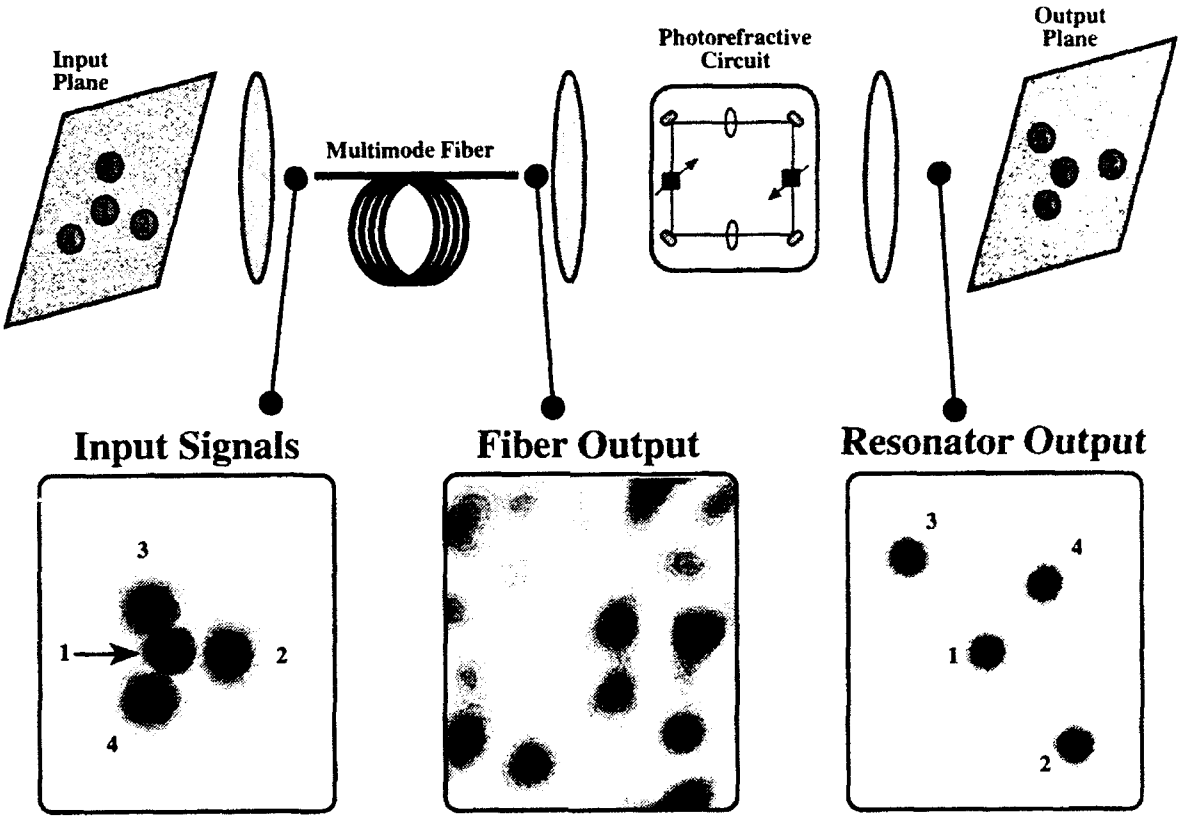

In future work we intend to redesign the optical system towards better mapping properties. It is clear that the wandering spot behavior is essentially unavoidable, since misalignments of the resonator may be made small but they will always be finite. Furthermore, our theoretical work has indicated that in order to enforce greater spatial stability, a stronger transverse interaction must take place within the nonlinearity. That is, if one were to think of the imaging resonator for the moment as a collection of discrete resonators, we require greater competitive interaction among the distinct resonators. Currently, the interaction occurs only indirectly, through competition for gain (or for less loss) in the nonlinear media. One can achieve the desired transverse interaction using a third photorefractive element and a holographic element which

allows each point in the transverse plane to nonlinearly directly interact with every other point. The nonlinearity is provided by the third photorefractive medium, the transvere structure of the interaction (how much each point interacts with every other point) is controlled by the holographic element.

References

1. T. Kohonen, *Self-Organization and Associative Memory*. T. S. Huang, T. Kohonen, M. R. Schroeder, Eds., Information Science (Springer-Verlag, Berlin, 1989).

2. V. I. Bespalov, V. I. Talanov, *Pis'ma Zh. Eksp Theor. Fiz.* **3**, 471 (1966).

3. S. N. Vlasov, V. I. Talanov, in *Optical Phase Conjugation in Nonlinear Media* V. I. Bespalov, Eds. (USSR Academy of Sciences, Gorki, USSR, 1979) pp. 85.

4. S. N. Vlasov, E. V. Sheinina, *Radiophys. Quant. Electron.* **27**, 293 (1983).

5. L. A. Lugiato, *Phys. Rep.* **219**, 293 (1992).

6. C. O. Weiss, *Phys. Rep.* **219**, 311 (1992).

7. G. Grynberg, et al., *Opt. Comm.* **67**, 363 (1988).

8. M. Saffman, D. Montgomery, D. Z. Anderson, OSA Topical Metting on Nonlinear Dynamics in Optical Systems Alpbach, Austria, 1992),

9. D. M. Lininger, P. J. Martin, D. Z. Anderson, *Opt. Lett.* **14**, 697 (1989).

10. D. M. Lininger, D. D. Crouch, P. J. Martin, D. Z. Anderson, *Opt. Comm* **76**, 89 (1990).

11. J. A. Arnaud, *Appl. Opt.* **8**, 189 (1969).

12. R. Macdonald, H. J. Eichler, *Opt. Commun.* **89**, 289 (1992).

13. G. D'Alessandro, W. J. Firth, *Phys. Rev. Lett.* **66**, 2597 (1991).

14. N. V. Kukhtarev, V. B. Markov, S. G. Odulov, M. S. Soskin, V. L. Vinetskii, *Ferroelectrics* **22**, 949 (1979).

15. T. Honda, *To appear in Opt. Lett.* , (1993).